

Curie temperature of emerging two-dimensional magnetic structuresXiaobo Lu,¹ Ruixiang Fei,¹ and Li Yang^{1,2}¹*Department of Physics, Washington University in St. Louis, St. Louis, Missouri 63130, USA*²*Institute of Materials Science and Engineering, Washington University in St. Louis, St. Louis, Missouri 63130, USA*

(Received 3 August 2019; published 7 November 2019)

Recent realizations of intrinsic, long-range magnetic orders in two-dimensional (2D) van der Waals materials have ignited tremendous research interest. In this work, we employ the XXZ Heisenberg model and Monte Carlo simulations to study a fundamental property of these emerging 2D magnetic materials, the Curie temperature (T_c). By including both on-site and neighbor couplings extracted from first-principles simulations, we have calculated T_c of monolayer chromium trihalides and $\text{Cr}_2\text{Ge}_2\text{Te}_6$, which are of broad interest currently, and the simulation results agree with available measurements. We also clarify the roles played by anisotropic and isotropic interactions in deciding T_c of magnetic orders. Particularly, we find a universal, linear dependence between T_c and magnetic interactions within the parameter space of realistic materials. With this linear dependence, we can predict T_c of general 2D lattice structures, omitting the Monte Carlo simulations. Compared with the widely used Ising model, mean-field theory, and spin-wave theory, this work provides a convenient and quantitative estimation of T_c , giving hope to speeding up the search for novel 2D materials with higher Curie temperatures.

DOI: [10.1103/PhysRevB.100.205409](https://doi.org/10.1103/PhysRevB.100.205409)**I. INTRODUCTION**

Long-range magnetic orders had been believed to hardly survive in two-dimensional (2D) systems due to the enhanced thermal fluctuations that make spontaneously symmetry-breaking orders unsustainable [1,2]. In the 1960s, the Mermin-Wagner (MW) theorem showed that such symmetry-breaking order states are only ruled out if considering continuous rotational symmetries and short-range interactions, indicating the existence of 2D magnetism with anisotropic interactions [3–5]. The recent discoveries of 2D magnetic crystals confirmed that magnetic anisotropy plays a crucial role in realizing 2D ferromagnetism [5–8]. With the help of magnetic anisotropy, the long-range ferromagnetic (FM) order could be established in 2D structures by opening a magnon gap to resist the thermal agitation [7,9–11]. In early 2017, the ferromagnetic (FM) order in pristine 2D crystals was observed in both monolayer CrI_3 and $\text{Cr}_2\text{Ge}_2\text{Te}_6$ (CGT), and great enthusiasm has been aroused for searching and exploring 2D magnetism [6,7]. More recently, many other 2D magnetic materials, e.g., FePS_3 [12,13], Fe_3GeTe_2 [14,15], VSe_2 [16], MnSe_2 [17], and MnBi_2Te_4 [18,19], have been realized by either exfoliation from bulk structures or growth with molecular beam epitaxy (MBE). Interesting magnetic properties, such as room-temperature intrinsic ferromagnetism [16], magnetic topological insulators [18,19], and electric-field/doping tunable magnetism [20–22], etc., have been observed in these newborn 2D magnetic materials.

The most important character of ferromagnetism is the phase-transition temperature, i.e., the Curie temperature (T_c), which not only decides applications but also reflects the intrinsic magnetic mechanism. To date, numerous theoretical calculations have focused on this important magnetic property [23]. Take the intensively studied monolayer CrI_3 as an example. The experimentally measured value is around

45 K [6]. The Ising model predicted an overrated T_c over 80 K [24,25] because of the overestimation of anisotropic interactions. The spin-wave theory gave a better estimation of 33 K [25]. However, the harmonic and mean-field approximations in the spin-wave Hamiltonian and the corresponding magnetization introduce extra error bars. A few Monte Carlo (MC) simulations predicted T_c in a range between 50 and 96 K, depending on their parameters and Hamiltonians [26,27]. Importantly, recent studies [28–30] not only show the reliability of MC simulations compared with the random phase approximation, but further reveal direct relations between T_c and corresponding magnetic interaction strengths. Therefore, along this direction, more works are necessary for theoretically calculating reliable T_c of those 2D magnetic structures and understanding anisotropic magnetic interactions and their impacts on 2D magnetism.

In this work, we start from the XXZ Heisenberg model with the magnetic interaction parameters extracted from first-principles simulations. By using the MC simulation, we obtain the T_c of the widely studied monolayer chromium trihalides and CGT. Our result of monolayer CrI_3 is around 42 K, which is in excellent agreement with the measurement (45 K). More interestingly, we find that there is a universal, linear dependence between T_c and magnetic interaction coefficients within a wide range of parameter space. As a result, we can conveniently predict T_c of 2D Heisenberg-type magnetic materials based on the magnetic interactions without time-consuming MC simulations. Using the MC-simulated magnetic phase diagram, we explain the origin of such a linear relation and show the crucial role of anisotropic magnetic interactions in creating and keeping 2D magnetism. This advance can be useful for quantitatively understanding the origin of 2D magnetism and speeding up the discovery of novel 2D magnetic materials.

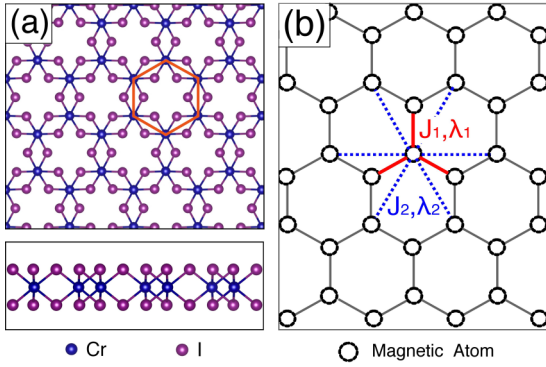


FIG. 1. (a) The top and side views of the atomic structure of monolayer CrI_3 . The magnetic Cr atoms form hexagonal lattices. (b) The XXZ model applies to hexagonal lattices. Each site has a localized magnetic moment, and the NN and NNN coupling interactions are indicated.

The article is organized in the following order. In Sec. II, we present the atomic structures of our studied 2D magnetic materials and first-principles simulation setups. In Sec. III, we introduce the XXZ Heisenberg model and MC simulations. In Sec. IV, the MC simulation results based on the XXZ Heisenberg model are presented and compared with measurements. In Sec. V, we reveal the linear dependence of the T_c on magnetic interactions. In Sec. VI, we discuss the phase diagram of 2D magnetism according to the anisotropic on-site and exchange interactions to understand the linear dependence and the roles played by anisotropic magnetic interactions. In Sec. VII, we summarize the results.

II. ATOMIC STRUCTURE AND FIRST-PRINCIPLES SIMULATION SETUPS

DFT calculations. The DFT calculations are performed within the generalized gradient approximation (GGA) using the Perdew-Burke-Ernzerhof (PBE) functional implemented in the Vienna *Ab Initio* Simulation Package (VASP) [31,32]. A plane-wave basis set with a kinetic energy cutoff of 450 eV and a $5 \times 5 \times 1$ k -point sampling grid are adopted for a $2 \times 2 \times 1$ supercell to mimic different magnetic configurations for extracting magnetic interactions. The vacuum distance is set to be 20 Å between adjacent layers to avoid spurious interactions. The van der Waals (vdW) interaction is included by the DFT-D2 method, [33] and spin-orbit coupling (SOC) is always considered. We choose the Hubbard $U = 2.7$ eV and Hund $J = 0.7$ eV parameters for Cr^{3+} ions, which have been widely used in previous works [24,25,34]. The geometric structure is relaxed until the force converged within 0.01 eV/Å.

Atomic structure. Monolayer chromium trihalides and CGT share a similar lattice structure. Take monolayer CrI_3 as an example. As shown in Fig. 1(a), Cr^{3+} cations are arranged in honeycomb lattices while carrying the localized magnetic moments ($3\mu_B/\text{Cr}^{3+}$), and they are coordinated to six nearest-neighbor I^- anions, forming an edge-sharing octahedral. By maintaining the C_3 rotational symmetry, our fully relaxed in-plane lattice constant is 6.91 Å, which well agrees with previous published results [24,27].

III. HEISENBERG MODEL AND MC SIMULATION SETUP

The Heisenberg model is a widely employed approach to study 2D magnetism since the early works by Mermin and Wagner [1–4]. The Heisenberg formalism provides enriched stages for various physics phenomena in 2D magnetism, such as quantum critical behavior and nontrivial phase transitions, i.e., the Berezinskii-Kosterlitz-Thouless (BKT) transition in 2D Heisenberg model with easy-plane anisotropy [3,4,35,36]. Previous works showed that 2D magnetic materials, such as monolayer CrI_3 , exhibit an easy axis along the out-of-plane direction, and the magnetic energy is approximately isotropic along in-plane directions, making it reasonable to further mutate the Heisenberg model into a quantum anisotropic Heisenberg model, also called the XXZ model [6,25,37,38].

In this work, we construct the XXZ Hamiltonian by including both on-site and coupling anisotropic magnetic interactions as follows:

$$\mathcal{H} = \sum_i A(S_i^z)^2 + \sum_{\langle i,j \rangle} \frac{1}{2} (\lambda_1 S_i^z S_j^z + J_1 \vec{S}_i \cdot \vec{S}_j) + \sum_{\langle\langle i,j \rangle\rangle} \frac{1}{2} (\lambda_2 S_i^z S_j^z + J_2 \vec{S}_i \cdot \vec{S}_j). \quad (1)$$

As indicated in Fig. 1(b), the interactions among those highly localized magnetic moments can be reasonably described by neighbor couplings which include both isotropic exchange interaction J and anisotropic exchange coupling λ . The subscript 1 means the nearest-neighbor (NN) coupling, and the subscript 2 means the next NN (NNN) coupling. The coefficient A describes the easy-axis, single-ion anisotropy. In this work, we neglect the third NN and farther couplings because they are an order of magnitude smaller [27,38].

To obtain the phase transition and T_c , we perform MC simulations based on the Metropolis algorithm on 2D hexagonal lattices with a size of 40×40 unit cells, which contain 3200 magnetic moments. The periodic boundary condition is implemented. A MC step consists of an attempt to assign a new random direction in 3D space to one of the random magnetic moments in the lattices. All magnetic moments point along the out-of-plane direction at the initial state to mimic experimental setups, in which the low-temperature ground state is obtained under external assisting magnetic fields [6,7,39,40]. We run for 4×10^8 MCs (2.5×10^5 steps per site average) to ensure that the thermal equilibrium is achieved. For each temperature point, there are 20 independent runs to reduce the statistical fluctuation.

The magnetization is defined as

$$\langle m_\alpha \rangle = \frac{1}{N} \sum_{i=1}^N \langle S_i^\alpha \rangle, \quad (2)$$

where N represents the total magnetic moments in the simulated system, and $\langle S_i^\alpha \rangle$ indicates the time average of corresponding magnetic components after the simulation achieves thermal equilibrium. Finally, T_c can be estimated by fitting the typical phase-transition formula:

$$\langle m_z \rangle = \begin{cases} \mu(T_c - T)^\delta, & T_c > T \\ 0, & T_c < T \end{cases} \quad (3)$$

TABLE I. Extracted magnetic interaction parameters of Eq. (1), T_c of MC simulations, linear-model estimations, and experimental measurements. The unit of parameters is meV.

	A	λ_1	J_1	λ_2	J_2	MC T_c (K)	Model T_c (K)	Expt. T_c (K) monolayer	Expt. T_c (K) bulk
CrI ₃	-0.087	-0.085	-2.12	0.02	-0.35	42.2	42.8	45 K [6]	61 K [39]
CrBr ₃	-0.02	-0.016	-1.35	-0.001	-0.153	23.1	24.0	27 K [42]	37 K [51]
CrCl ₃	-0.007	-0.002	-0.79	0	-0.071	12.1	13.1	17 K (2 L) [42,43]	17 K [40]
Cr ₂ Ge ₂ Te ₆	-0.01		-2.71		0.0058		34.5	30 K (2 L) [7]	68 K [7]

IV. MAGNETIC PHASE TRANSITION AND T_c

First, we must obtain the coefficients of magnetic interactions in the Hamiltonian of Eq. (1) by calculating total energies of different magnetic configurations. Here we consider the FM and Néel antiferromagnetic (AFM) configurations. The corresponding energy expressions of a unit cell are

$$E_{\text{FM/AFM}}^{\text{out}} = E_0 + (2A \pm 3\lambda_1 \pm 3J_1 + 6\lambda_2 + 6J_2)S^2, \quad (4)$$

$$E_{\text{FM/AFM}}^{\text{in}} = E_0 + (\pm 3J_1 + 6J_2)S^2, \quad (5)$$

in which two magnetic orientations (in-plane and out-of-plane ones) are calculated in order to specify anisotropic couplings. Moreover, we can flip the magnetic moment of a Cr³⁺ cation in a $2 \times 2 \times 1$ supercell to obtain more energy configurations (normalized to one unit cell).

$$E_{\text{flip}}^{\text{out}} = E_0 + (2A + \frac{3}{2}\lambda_1 + \frac{3}{2}J_1 + 3\lambda_2 + 3J_2)S^2, \quad (6)$$

$$E_{\text{flip}}^{\text{in}} = E_0 + (\frac{3}{2}J_1 + 3J_2)S^2. \quad (7)$$

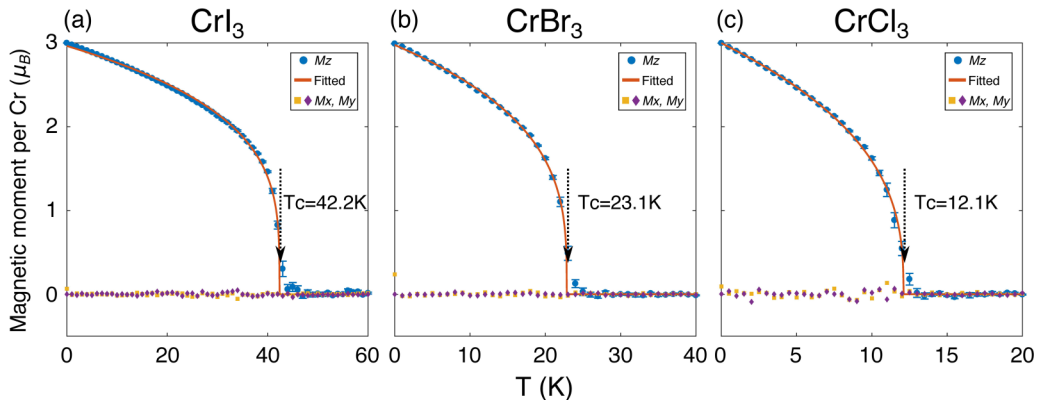
As a result, we accumulate six equations that can solve the five magnetic interaction coefficients in Eq. (1) and reference energy (E_0).

The magnetic interaction coefficients, which are extracted from DFT calculations, of monolayer chromium trihalides are summarized in Table I. As expected, the isotropic NN coupling (J_1) is the strongest and has a negative sign, resulting in the FM ground state. Both the signs of the anisotropic NN coupling (λ_1) and on-site anisotropic term (A) are negative, indicating the easy axis of magnetization is along the z (out-of-plane) direction. Importantly, anisotropic interactions are significantly weaker than isotropic ones. For example, the isotropic NN coupling J_1 is about -2.12 meV for monolayer CrI₃, and the anisotropic NN coupling λ_1

is about -0.085 meV. These results are close to previous published results [25]. Finally, as discussed in previous works, magnetic interactions of these monolayer structures are mainly from halogen-atom SOC mediated superexchange interactions between Cr³⁺ cations [25,41]. Therefore, we observe that magnetic interactions are reduced from CrI₃ to CrBr₃ to CrCl₃, along the trend of lighter halogen atoms.

With these magnetic coupling coefficients, we can obtain the dependence of magnetization according to temperature by MC simulations in Fig. 2. Magnetic phase transitions are observed, and T_c is 42.2, 23.1, and 12.1 K for monolayer CrI₃, CrBr₃, and CrCl₃, respectively. To date, the measured Curie temperatures of monolayer CrI₃ and CrBr₃ are around 45 and 27 K, respectively [6,42]. Compared with previous results from the Ising model, mean-field theory, and spin-wave theory, our calculation agrees better with measurements. For CrCl₃, the available measurement of the two-layer (2-L) structure is about 17 K which is slightly higher than our predicted T_c (12 K) of monolayer. This difference may be resulted from interlayer couplings of bilayer structures [42,43]. We have to address that these results are sensitive to the choices of U and J . As shown in previous works [28–30], different values of these two parameters will change the calculated T_c because the magnetic interactions are changed accordingly.

It must be pointed out that, although the NNN coupling J_2 is significantly smaller than J_1 , its contribution to T_c is not small due to the larger coordinate number of the next NN in hexagonal lattices ($N_2 = 6$). For chromium trihalides, we find that including the NNN coupling raises T_c by roughly 20%–30%. It is also worth pointing out that the anisotropy of both on-site energy and exchange interaction in CrCl₃ is quite weak. In such weakly anisotropic cases, the help of a small external field may be needed to observe the FM phase


 FIG. 2. The MC-simulated magnetism vs temperature for monolayer CrX₃ ($X = I, \text{Br}, \text{Cl}$) with the error bar.

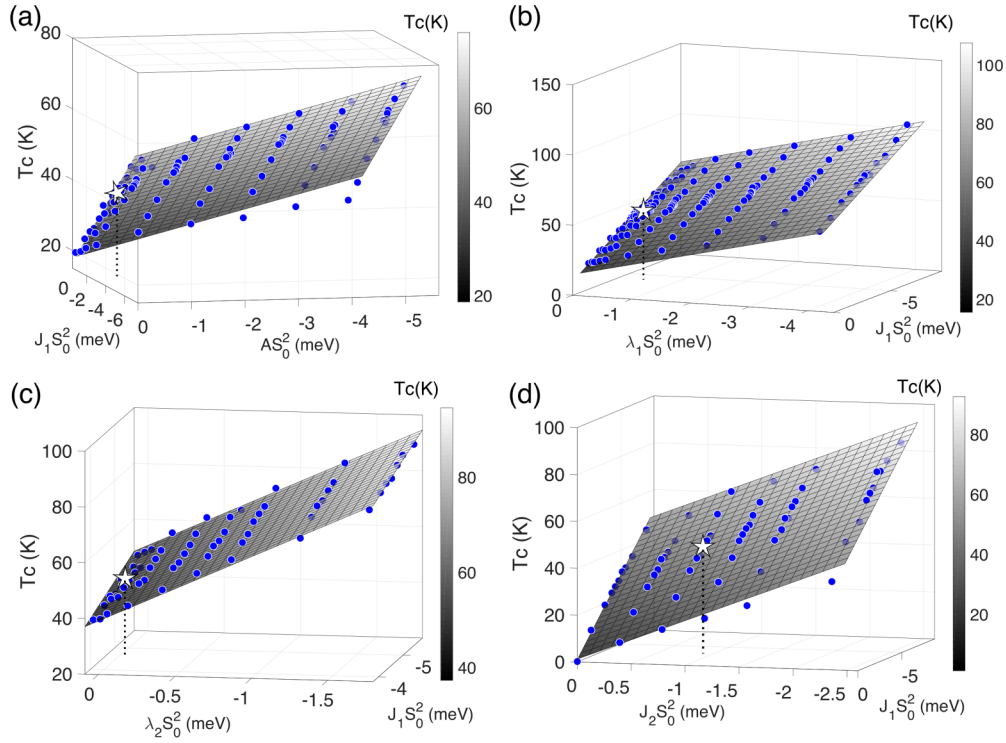


FIG. 3. The fitted linear relation between T_c and corresponding parameters of the XXZ model of 2D hexagonal lattices. The MC simulation points are solid blue points. (a–d) are the linearly fitted planes for corresponding on-site anisotropic A and NN isotropic, J_1 NN anisotropic coupling λ_1 and J_1 , NNN anisotropic coupling λ_2 and J_1 , and NNN isotropic coupling J_2 and J_1 , respectively. The corresponding parameters of monolayer CrI_3 are marked as white stars.

transition. This is similar to what has been discussed in the CGT experiment [7].

V. RELATIONSHIPS BETWEEN T_c AND MAGNETIC INTERACTION

Although MC simulations provide a good solution to the XXZ Hamiltonian, it is time consuming and complicated for spreading out to specific materials that use combinations of parameters. Since the magnetic energy and T_c are fundamentally decided by magnetic interactions, it will be interesting to explore if there is a direct relation between T_c and those interaction coefficients.

For this purpose, we scan a much larger parameter space by MC simulations based on the XXZ Heisenberg model [Eq. (1)]. However, we have five parameters, i.e., A , J_1 , J_2 , λ_1 , and λ_2 . It is impossible to cover such a five-dimensional parameter space, and we must simplify the scanning space. For most magnets, the NN isotropic coupling J_1 is usually the dominant factor for the amplitude of T_c . Therefore, we carry out extensive MC simulations by varying J_1 and one of other parameters from A , λ_1 , λ_2 , and J_2 while fixing the rest (e.g., at values of monolayer CrI_3). The results are shown in Fig. 3. Surprisingly, we find that T_c for each J_1 vs α ($\alpha = A, \lambda_1, \lambda_2, J_2$) is roughly sitting in a flat plane. It indicates that T_c of such an XXZ Heisenberg model is linearly dependent with these coupling strengths. This qualitatively agrees with the expressions in Refs. [28,29], which are based on the Ising limit value with NN couplings included.

T_c can be expressed as

$$k_B T_c = (\alpha_0)AS^2 + (\alpha_1^z n_1)\lambda_1 S^2 + (\alpha_1 n_1)J_1 S^2 + (\alpha_2^z n_2)\lambda_2 S^2 + (\alpha_2 n_2)J_2 S^2. \quad (8)$$

The NN and NNN coordinate number, n_i , and fitted values, α_i , are listed in Table II. With this linear dependence, we can predict T_c of 2D magnets without the MC simulation. As shown in Table I, this model predicting T_c is very close to MC results with an error bar of less than 1 K for monolayer chromium trihalides. We have tried this model with another family of 2D magnets, CGT, which has similar hexagonal structures as chromium trihalides. Using the published magnetic interaction coefficients [7], our estimated T_c of monolayer CGT is 34.5 K, which is kind of close to the available measured value (around 30 K under a 0.075-T external field) of bilayer CGT [7]. It has to be pointed out that, according to the MW theorem, this expression is no longer valid when all the anisotropy parameters approach zero. Fortunately, such an invalid region is small owing to the logarithmically asymptotical behavior of T_c , which will be discussed in Sec. VI.

TABLE II. Extracted coefficients of the linear model in Eq. (8) based on MC simulations.

	$\alpha_0 (A)$	$\alpha_1^z (\lambda_1)$	$\alpha_1 (J_1)$	$\alpha_2^z (\lambda_2)$	$\alpha_2 (J_2)$	n_1	n_2
Hexagonal	-0.33	-0.28	-0.164	-0.35	-0.256	3	6
Square	-0.34	-0.29	-0.183	-0.35	-0.257	4	4

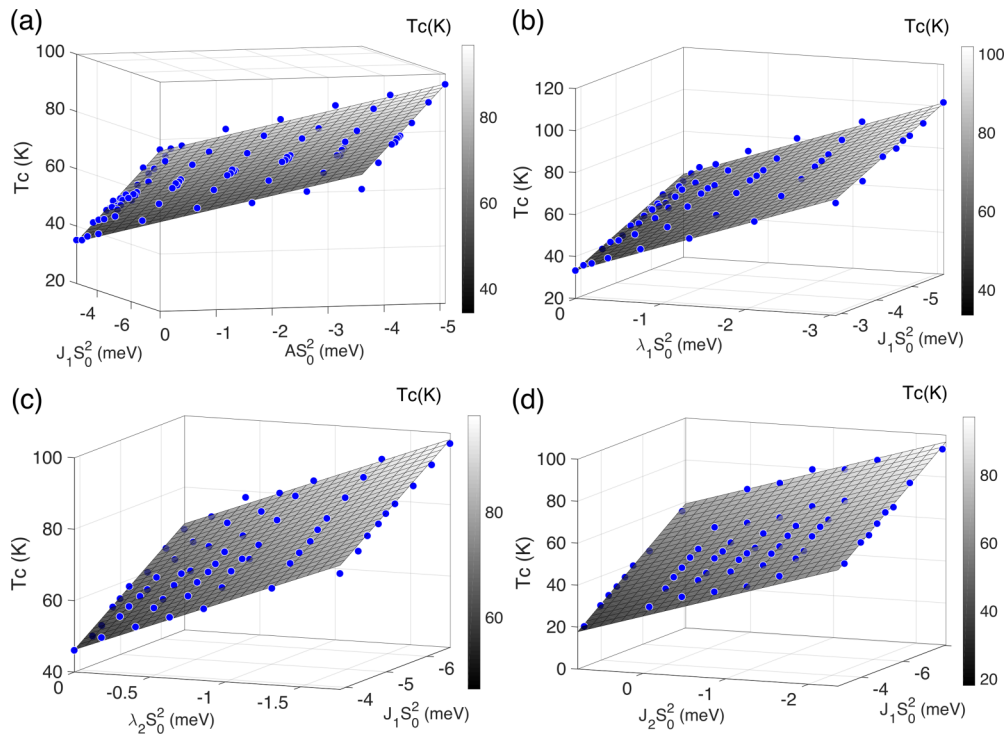


FIG. 4. The fitted linear relation between T_c and corresponding parameters of the XXZ model of 2D square lattices. The MC simulation points are solid blue points. (a–d) are the linearly fitted planes for corresponding on-site anisotropic A and NN isotropic J_1 , NN anisotropic coupling λ_1 and J_1 , NNN anisotropic coupling λ_2 and J_1 , and NNN isotropic coupling J_2 and J_1 , respectively.

Beyond hexagonal lattices, we also imitate the same processing of MC simulations on 2D square lattices by the XXZ Hamiltonian. As shown in Fig. 4, T_c for each J_1 vs α ($\alpha = A, \lambda_1, \lambda_2, J_2$) is roughly sitting in a flat plane. Therefore, similar linear dependence is concluded, and the extracted values of parameters of square lattices are listed in Table II. Interestingly, the coefficients of the linear model for both square and hexagonal lattices are similar to those shown in Table II. Therefore, this linearity is robust for different lattices, and the T_c expression [Eq. (8)] could be universal for anisotropic 2D XXZ Heisenberg systems.

In fact, a linear dependence of T_c according to the magnetic coupling coefficients has been proposed in other-level models [44]. For instance, it can be derived from the Hamiltonian in Eq. (1) that the widely used mean-field approximation (MFA) gives the linear relation [44]

$$T_c = \frac{2S(S+1)}{3k_B} \left(-A - \frac{n_1}{2}J_1 - \frac{n_1}{2}\lambda_1 - \frac{n_2}{2}J_2 - \frac{n_2}{2}\lambda_2 \right). \quad (9)$$

However, there are several obvious deficiencies in that MFA result. Firstly, the MFA cannot distinguish isotropic and anisotropic couplings due to the fact that all operators are replaced by their thermodynamic mean values along the out-of-plane direction. As a result, the slopes of the linear dependence are the same for both isotropic J and anisotropic λ . This overestimated anisotropy is a main reason for the much larger T_c provided by the MFA. In other words, MFA shall be appropriate for very strongly anisotropic magnetic systems.

Second, T_c is proportional to $S(S+1)$ in the MFA but our model shows that T_c is proportional to S^2 . This discrepancy originates from the different quantum and classic treatments

of the spin operator. To verify this point, we change the magnetic moment in MC simulations. Meanwhile, we tune the coupling constants simultaneously to keep the value of the product of $\alpha S_i^{(z)} S_j^{(z)}$ ($\alpha = A, \lambda, J$). In Fig. 5, the simulation shows that T_c does not change for different magnetic moments. For instance, the curve starting from $3\mu_B$ is simulating monolayer CrI_3 which has a magnetic moment of $m = 3\mu_B$ ($S = \frac{3}{2}$). If we reduce the magnetic moment to $1\mu_B$ ($S = 1/2$)

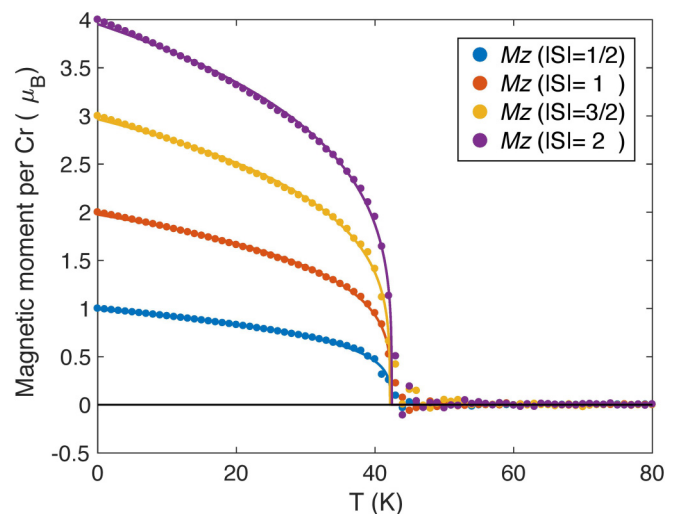


FIG. 5. The MC-simulated magnetism vs temperature for different magnetic-moment systems. The products $\alpha S_i^{(z)} S_j^{(z)}$ ($\alpha = A, \lambda, J$) are fixed at the same value for different magnetic moments.

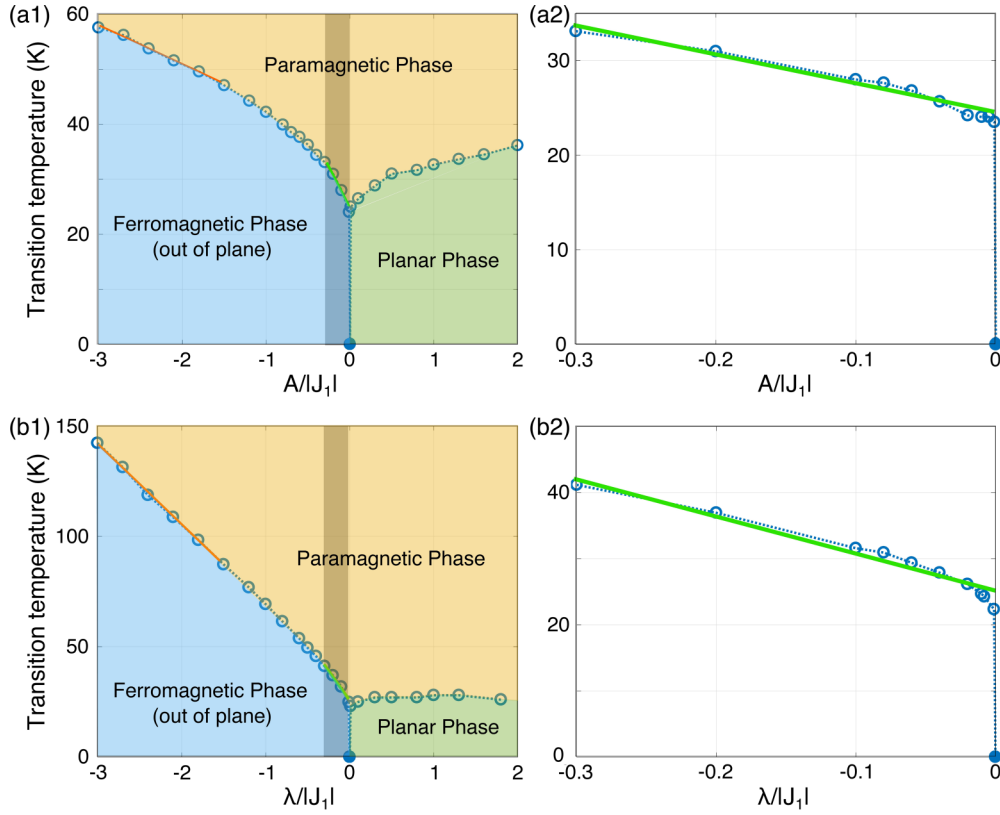


FIG. 6. (a1,b1) are phase diagrams generated from MC simulations of the Hamiltonian of Eqs. (10) and (11), respectively. The open circles are MC-simulated phase boundaries. (a2,b2) are amplified from the shaded area with more data points.

and increase all coupling strengths by 9 times to keep $\alpha S_i^{(z)} S_j^{(z)}$ as a constant, the calculated T_c does not change at all. This finding confirms the square relation between T_c and magnetic moment. In fact, similar behavior was also noticed in previous studies about ferroelectricity of monolayer group-IV monochalcogenides [45]. In this sense, our extracted model Eq. (8) can be suitable for general 2D anisotropic Heisenberg systems for both magnetic and electric polarizations, except the $S = \frac{1}{2}$ systems with only the single-ion anisotropy ($\lambda = 0$). Their spin-wave spectrum remains gapless, and magnetic orders may not be maintained, which cannot be captured by classic MC simulations [28,29].

VI. PHASE DIAGRAM OF THE ANISOTROPIC INTERACTIONS

There is an obvious question about the linear expression of Eq. (8): The different magnetic interactions contribute to T_c independently. This cannot be true for the whole parameter space. The extreme example is that when the anisotropic interactions are zero, that formula still gives a finite T_c . This obviously conflicts with the MW theorem [1,46]. In other words, this linear expression can only be true within a suitable regime (parameter space). To clarify this point, we study the phase diagram within a much larger parameter space, particularly for the small anisotropic regimes.

To address essential physics and avoid unnecessary complexity of scanning high-dimensional parameter space, we

focus on two simplified XXZ Heisenberg models:

$$\mathcal{H}_a = \sum_i A(S_i^z)^2 + \sum_{\langle i,j \rangle} \frac{1}{2} (J \vec{S}_i \cdot \vec{S}_j), \quad (10)$$

$$\mathcal{H}_b = \sum_{\langle i,j \rangle} \frac{1}{2} (\lambda_1 S_i^z S_j^z + J_1 \vec{S}_i \cdot \vec{S}_j). \quad (11)$$

The first one [Eq. (10)] focuses on how the on-site anisotropy impacts magnetic phases, while the second one [Eq. (11)] focuses on how the anisotropic coupling impacts magnetic phases. The MC results are presented in Fig. 6. Both models exhibit a similar phase diagram. There are basically three phases: the out-of-plane FM phase, the paramagnetic (PM) phase, and the planar phase. The planar phase is from the positive sign of the anisotropic terms, which drive magnetization from the out-of-plane easy axis (z) to the easy ($x - y$) plane. In the following, we mainly focus on the out-of-plane FM and PM phases, in which the sign of the anisotropic terms is negative.

The most striking part in the phase diagram of Fig. 6 is how the anisotropic term (A or λ) approaches zero. The MW theorem shows that anisotropy is necessary for holding the long-range magnetic order, while it does not answer how the anisotropy quantitatively impacts T_c . In Fig. 6, it shows that a minor anisotropy can dramatically, nonlinearly increase T_c . Our simulated behaviors around a perfect isotropic point agree with previous scalings [47] and renormalization group [48] analysis, in which T_c approaches zero logarithmically as the anisotropic term decreases [49,50]. In this sense, anisotropy

works as a seed to create the thermodynamically stable magnetic order while other couplings can further enhance the magnetic order. Due to this sharp variation, the region of divergence which adjoins the isotropic point is extremely small. Even if we take $\frac{\alpha}{|J_1|} \sim -0.001$ ($\alpha = A, \lambda$), our MC simulation still exhibits a nonzero T_c .

On the other hand, this sharp nonlinear region is so narrow that it provides a good chance for estimating T_c by the first-order linear approximation within a reasonable region. More specifically, for most 2D magnetic materials, the amplitudes of anisotropic terms are substantially smaller than that of the isotropic NN coupling (J_1), as shown in Table I. Therefore, the true material parameter space is very narrow, which is in the gray-colored space in Figs. 6(a1) and 6(b1). We amplify that regime and observe a very good linear relation in Figs. 6(a2) and 6(b2). This is why we obtain the linear relation between T_c and magnetic couplings in Figs. 3 and 4. Finally, in Figs. 6(a1) and 6(b1), when the anisotropy is very large (the far-left side), we approach the MFA limit discussed in Sec. V. A linear relation is also observed but with different slopes from that of realistic materials marked by gray-colored space).

Finally, we must point out that the values of magnetic interactions, i.e., A, J , and λ , are crucial for deciding the value of T_c , as seen in Eq. (8). Unfortunately, it is known that it is challenging to accurately calculate those magnetic interaction coefficients of correlated materials by *ab initio* approaches. Therefore, how to obtain reliable magnetic interactions is the fundamental challenge for studying these materials and MC simulations, and this is beyond the scope of this work. On the other hand, our proposed linear model survives in a wide

range of parameter space (Figs. 3 and 4), making it robust as long as reliable magnetic interactions are obtained.

VII. CONCLUSIONS

In this work, we have calculated the Curie temperature T_c of the widely studied monolayer chromium trihalides and CGT by MC simulations based on the XXZ model with magnetic interactions extracted from first-principles calculations. Our calculated T_c of monolayer CrI_3 agrees excellently with measurements. Moreover, we find a universal, linear dependence between T_c and magnetic interactions within the parameter space of realistic materials. With this linear dependence, we can predict T_c of 2D magnets without MC simulations once we have obtained reliable magnetic interactions. This linear model provides insights to clarify and understand the roles of isotropic and anisotropic magnetic interactions in deciding T_c : The anisotropic terms typically ensure the stability for the FM order in 2D magnets, and isotropic terms basically decide the magnitude of T_c . It also sheds light on searching for novel 2D materials with higher Curie temperatures by engineering the anisotropic and isotropic magnetic interactions.

ACKNOWLEDGMENTS

The work is supported by the National Science Foundation (NSF) CAREER Grant No. DMR-1455346 and the Air Force Office of Scientific Research (AFOSR) Grant No. FA9550-17-1-0304. The computational resources have been provided by the Stampede of TeraGrid at the Texas Advanced Computing Center (TACC) through XSEDE.

-
- [1] N. D. Mermin and H. Wagner, *Phys. Rev. Lett.* **17**, 1133 (1966).
 - [2] P. C. Hohenberg, *Phys. Rev.* **158**, 383 (1967).
 - [3] J. M. Kosterlitz and D. J. Thouless, *J. Phys. C: Solid State Phys.* **6**, 1181 (1973).
 - [4] J. V. José, L. P. Kadanoff, S. Kirkpatrick, and D. R. Nelson, *Phys. Rev. B* **16**, 1217 (1977).
 - [5] P. Bruno, *Mater. Res. Soc. Symp. Proc.* **231**, 299 (1991).
 - [6] B. Huang, G. Clark, E. Navarro-Moratalla, D. R. Klein, R. Cheng, K. L. Seyler, D. Zhong, E. Schmidgall, M. A. McGuire, D. H. Cobden, W. Yao, D. Xiao, P. Jarillo-Herrero, and X. Xu, *Nature* **546**, 270 (2017).
 - [7] C. Gong, L. Li, Z. Li, H. Ji, A. Stern, Y. Xia, T. Cao, W. Bao, C. Wang, Y. Wang, Z. Q. Qiu, R. J. Cava, S. G. Louie, J. Xia, and X. Zhang, *Nature* **546**, 265 (2017).
 - [8] K. S. Burch, D. Mandrus, and J.-G. Park, *Nature* **563**, 47 (2018).
 - [9] C. Gong and X. Zhang, *Science* **363**, eaav4450 (2019).
 - [10] T. J. Williams, A. A. Aczel, M. D. Lumsden, S. E. Nagler, M. B. Stone, J.-Q. Yan, and D. Mandrus, *Phys. Rev. B* **92**, 144404 (2015).
 - [11] L. Chen, J.-H. Chung, B. Gao, T. Chen, M. B. Stone, A. I. Kolesnikov, Q. Huang, and P. Dai, *Phys. Rev. X* **8**, 041028 (2018).
 - [12] J.-U. Lee, S. Lee, J. H. Ryoo, S. Kang, T. Y. Kim, P. Kim, C.-H. Park, J.-G. Park, and H. Cheong, *Nano Lett.* **16**, 7433 (2016).
 - [13] X. Wang, K. Du, Y. Y. Fredrik Liu, P. Hu, J. Zhang, Q. Zhang, M. H. S. Owen, X. Lu, C. K. Gan, P. Sengupta, C. Kloc, and Q. Xiong, *2D Mater.* **3**, 031009 (2016).
 - [14] Y. Deng, Y. Yu, Y. Song, J. Zhang, N. Z. Wang, Z. Sun, Y. Yi, Y. Z. Wu, S. Wu, J. Zhu, J. Wang, X. H. Chen, and Y. Zhang, *Nature* **563**, 94 (2018).
 - [15] Z. Fei, B. Huang, P. Malinowski, W. Wang, T. Song, J. Sanchez, W. Yao, D. Xiao, X. Zhu, A. F. May, W. Wu, D. H. Cobden, J.-H. Chu, and X. Xu, *Nat. Mater.* **17**, 778 (2018).
 - [16] M. Bonilla, S. Kolekar, Y. Ma, H. C. Diaz, V. Kalappattil, R. Das, T. Eggers, H. R. Gutierrez, M.-H. Phan, and M. Batzill, *Nat. Nanotechnol.* **13**, 289 (2018).
 - [17] D. J. O'Hara, T. Zhu, A. H. Trout, A. S. Ahmed, Y. K. Luo, C. H. Lee, M. R. Brenner, S. Rajan, J. A. Gupta, D. W. McComb, and R. K. Kawakami, *Nano Lett.* **18**, 3125 (2018).
 - [18] M. M. Otrokov, I. I. Klimovskikh, H. Bentmann, A. Zeugner, Z. S. Aliev, S. Gass, A. U. B. Wolter, A. V. Koroleva, D. Estyunin, A. M. Shikin, M. Blanco-Rey, M. Hoffmann, A. Y. Vyazovskaya, S. V. Eremeev, Y. M. Koroteev, I. R. Amiraslanov, M. B. Babanly, N. T. Mamedov, N. A. Abdullayev, V. N. Zverev *et al.*, [arXiv:1809.07389](https://arxiv.org/abs/1809.07389).

- [19] Y. Gong, J. Guo, J. Li, K. Zhu, M. Liao, X. Liu, Q. Zhang, L. Gu, L. Tang, X. Feng, D. Zhang, W. Li, C. Song, L. Wang, P. Yu, X. Chen, Y. Wang, H. Yao, W. Duan, Y. Xu *et al.*, *Chin. Phys. Lett.* **36**, 076801 (2019).
- [20] B. Huang, G. Clark, D. R. Klein, D. MacNeill, E. Navarro-Moratalla, K. L. Seyler, N. Wilson, M. A. McGuire, D. H. Cobden, D. Xiao, W. Yao, P. Jarillo-Herrero, and X. Xu, *Nat. Nanotechnol.* **13**, 544 (2018).
- [21] S. Jiang, J. Shan, and K. F. Mak, *Nat. Mater.* **17**, 406 (2018).
- [22] S. Jiang, L. Li, Z. Wang, K. F. Mak, and J. Shan, *Nat. Nanotechnol.* **13**, 549 (2018).
- [23] L. J. de Jongh and A. R. Miedema, *Adv. Phys.* **23**, 1 (1974).
- [24] J. Liu, Q. Sun, Y. Kawazoe, and P. Jena, *Phys. Chem. Chem. Phys.* **18**, 8777 (2016).
- [25] J. L. Lado and J. Fernández-Rossier, *2D Mater.* **4**, 035002 (2017).
- [26] C. Huang, J. Feng, F. Wu, D. Ahmed, B. Huang, H. Xiang, K. Deng, and E. Kan, *J. Am. Chem. Soc.* **140**, 11519 (2018).
- [27] W.-B. Zhang, Q. Qu, P. Zhu, and C.-H. Lam, *J. Mater. Chem. C* **3**, 12457 (2015).
- [28] D. Torelli and T. Olsen, *2D Mater.* **6**, 015028 (2018).
- [29] D. Torelli, K. S. Thygesen, and T. Olsen, *2D Mater.* **6**, 045018 (2019).
- [30] T. Olsen, *MRS Commun.* (2019), doi:10.1557/mrc.2019.117.
- [31] J. P. Perdew, K. Burke, and M. Ernzerhof, *Phys. Rev. Lett.* **77**, 3865 (1996).
- [32] G. Kresse and J. Furthmüller, *Phys. Rev. B* **54**, 11169 (1996).
- [33] S. Grimme, *J. Comput. Chem.* **25**, 1463 (2004).
- [34] P. Jiang, L. Li, Z. Liao, Y. X. Zhao, and Z. Zhong, *Nano Lett.* **18**, 3844 (2018).
- [35] A. V. Chubukov, S. Sachdev, and J. Ye, *Phys. Rev. B* **49**, 11919 (1994).
- [36] L. Wang, K. S. D. Beach, and A. W. Sandvik, *Phys. Rev. B* **73**, 014431 (2006).
- [37] L. Webster and J. A. Yan, *Phys. Rev. B* **98**, 144411 (2018).
- [38] F. Zheng, J. Zhao, Z. Liu, M. Li, M. Zhou, S. Zhang, and P. Zhang, *Nanoscale* **10**, 14298 (2018).
- [39] M. A. McGuire, H. Dixit, V. R. Cooper, and B. C. Sales, *Chem. Mater.* **27**, 612 (2015).
- [40] M. A. McGuire, G. Clark, Santosh KC, W. M. Chance, G. E. Jellison, Jr., V. R. Cooper, X. Xu, and B. C. Sales, *Phys. Rev. Mater.* **1**, 014001 (2017).
- [41] C. Xu, J. Feng, H. Xiang, and L. Bellaïche, *NPJ Comput. Mater.* **4**, 57 (2018).
- [42] H. H. Kim, B. Yang, S. Li, S. Jiang, C. Jin, Z. Tao, G. Nichols, F. Sfigakis, S. Zhong, C. Li, S. Tian, D. G. Cory, G.-X. Miao, J. Shan, K. F. Mak, H. Lei, K. Sun, L. Zhao, and A. W. Tsien, *Proc. Natl. Acad. Sci. USA* **116**, 11131 (2019).
- [43] X. Cai, T. Song, N. P. Wilson, G. Clark, M. He, X. Zhang, T. Taniguchi, K. Watanabe, W. Yao, D. Xiao, M. A. McGuire, D. H. Cobden, and X. Xu, *Nano Lett.* **19**, 3993 (2019).
- [44] K. Yosida, *Theory of Magnetism* (Springer Science & Business Media, Berlin, 1996).
- [45] R. Fei, W. Kang, and L. Yang, *Phys. Rev. Lett.* **117**, 097601 (2016).
- [46] H. W. J. Blöte, W. Guo, and H. J. Hilhorst, *Phys. Rev. Lett.* **88**, 047203 (2002).
- [47] S. Hikami and T. Tsuneto, *Prog. Theor. Phys.* **63**, 387 (1980).
- [48] R. A. Pelcovits and D. R. Nelson, *Phys. Lett. A* **57**, 23 (1976).
- [49] N. W. Dalton and D. W. Wood, *Proc. Phys. Soc.* **90**, 459 (1967).
- [50] C. Kawabata and A. R. Bishop, *Solid State Commun.* **42**, 595 (1982).
- [51] B. I. Tsubokawa, *J. Phys. Soc. Jpn.* **15**, 1664 (1960).